Chapter 8 Appendix 4

NEUTRON AND PHOTON FLUENCE-TO-DOSE CONVERSION FACTORS FOR ACTIVE MARROW OF THE SKELETON

George D. Kerr and Keith F. Eckerman
Oak Ridge National Laboratory

Calculation of absorbed dose in active marrow is a complex problem because charge-particle equilibrium may not exist near a soft-tissue/bone interface, and it is difficult to model the intricate intermixture of soft tissue and bone in the skeleton.[1–6] In previous calculations for neutrons and photons, specific geometrical models were used for the marrow cavities (e.g., thin slabs, cylinders, and spheres). These studies indicate clearly that the presence of bone alters the absorbed dose in active marrow from photons with energies below several hundred keV and neutrons with energies of several MeV or more, but the results cannot be applied generally. This study provides the first definitive calculations for a variety of active marrow sites in the skeleton and a wide range of neutron and photon energies. We avoid the assumption of a special geometry by using measured chord-length distributions to represent the microstructure of the trabecular bones containing the active marrow.[7–10] The results of our calculations for neutrons and photons with energies up to 20 MeV are presented as fluence-to-dose conversion factors, for application in radiation transport calculations of absorbed dose in active marrow from photons and neutrons externally incident on the body, and photons produced by neutron interactions within the body.

Geometrical Probability

Concepts of geometrical probability dealing with distributions of chord lengths in convex bodies have found wide application in such diverse fields as radiation dosimetry, image analysis, reactor design, ecology, and acoustics.[11–13] There are many ways in which the randomness of chords in a convex body may arise; however, only two are of interest here[13,14]

Mean free path randomness (or μ-randomness) results if a series of random points is selected uniformly outside a convex body and each point is an isotropic source of straight

lines.

Interior radiator randomness (or I-randomness) results if a series of random points is selected uniformly inside the convex body and each point is an isotropic source of straight lines.

The probability density functions of chord lengths, f(x), for μ- and I-randomness in a convex body are related as:[14,15]

$$f_I(x) = x f_\mu(x) / < x >_\mu \tag{1}$$

where <x> denotes the mean value of a probability density function. The mean value for μ-randomness is related to the volume, V, and surface area, A, of a convex body by Cauchy's theorem:[11]

$$< x >_\mu = 4V/A \tag{2}$$

We are dealing with μ-randomness when charged particles originate outside a convex body (e.g., a marrow cavity). If the charged particles originate inside the convex body, then I-randomness is applicable. The probability density function for I-randomness given in Equation 1 refers to a full chord, while the path length of a charged particle originating in a convex body is only a segment of the full chord. A full chord gives rise to a uniform distribution of path lengths, x, and the distribution of chord lengths for I-randomenss inside the convex body gives rise to a probability density function of path lengths, $f_i(x)$, which we denote as i-randomness. The function $f_i(x)$, given a distribution of i chord lengths, $f_I(x)$, is

$$f_i(x) = \int_x^\infty f_i(x \mid s) f_I(x) ds \tag{3}$$

where the conditional probability density function for a path length x, given a chord length s, is

$$f_i(x \mid s) = s^{-1}, 0 < x \leq s \tag{4}$$

By use of Equations 1, 3, and 4, we obtain

$$f_i(x) = [1 - F_\mu(x)] / < x >_\mu \tag{5}$$

where $F_\mu(x)$ is the cumulative probability density function:

$$F_\mu(x) = \int_0^x f_\mu(s)) ds \tag{6}$$

As an example, the chord-length distribution for μ-randomness in a spherical cavity of diameter d is simple and well-known:[16,17]

$$f_\mu(x) = 2x/d^2, < x >_\mu = 2d/3 \tag{7}$$

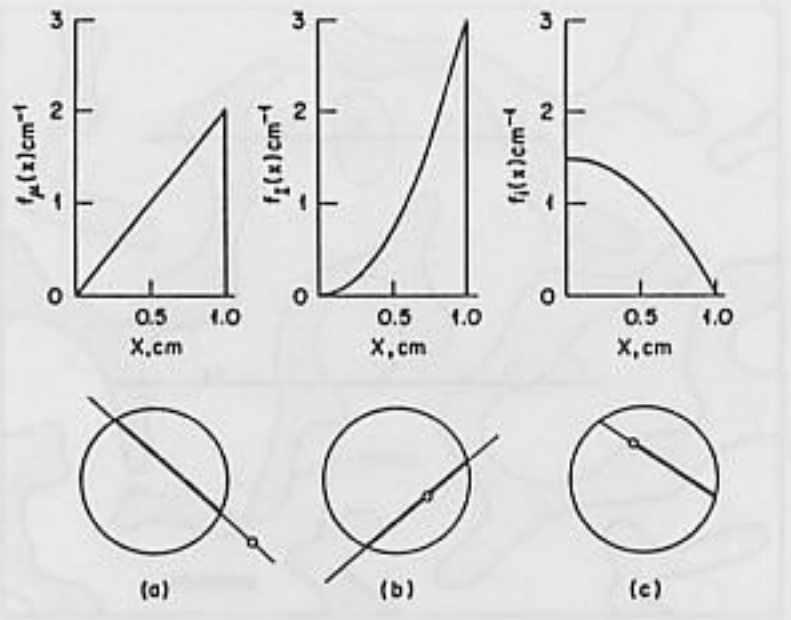

Figure 1. Distributions of chord lengths for (a) μ-randomness and (b) I-randomness, and (c) path lengths for i-randomness in a sphere with a diameter of one centimeter

By use of Equations 1 and 5 to 7, we obtain the following distributions for I-randomness of the chord lengths and i-randomness of the path lengths:

$$f_I(x) = 3x^2/d^3, f_i(x) = 3[1 - (x/d)^2]/2d \tag{8}$$

These various distributions are illustrated in Figure 1 for a sphere with a diameter of 1 cm. Suppose we need a path length from the distribution for i-randomness and know only the chord-length distribution for μ-randomness in a convex body. The first step would be to obtain the chord-length distribution for I-randomness using Equation 1, and by appropriate Monte Carlo sampling, we would select a full chord, and then a segment of the full chord using Equation 4. Hence, we can obtain the path lengths for charged particles originating uniformly and isotropically in a convex body given only the distribution for μ-randomness of the chord lengths.

Absorbed Fractions for Active Marrow

Consider a region of the body which absorbs energy from radiation emitted in another region. The effects of geometry and intervening materials on radiation transport between the two regions are embodied in calculations of the absorbed fractions, ϕ, defined as:[18,19]

$$\phi(v \leftarrow r) = \frac{\text{energy absorbed in target volume } v}{\text{energy emitted in source region } r} \tag{9}$$

We are interested in the active (red) marrow which is considered to be the critical tissue for induction of leukemia.[20] Thus, our absorbed-fraction data are developed with active marrow (or red marrow, RM) as the target volume, and the trabecular bone and active marrow (TB and RM) as source regions of monoenergetic charged particles (see Figure 2). The portion of a charged particle track crossing any marrow cavity or bone trabecula is represented

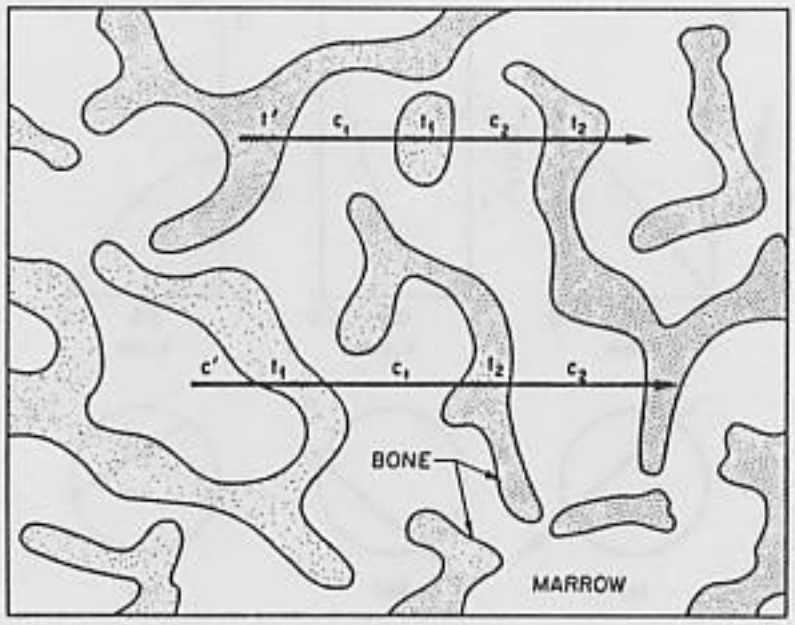

Figure 2. Illustration of typical tracks for charged particles originating in trabecular bone (top) and marrow cavities (bottom)

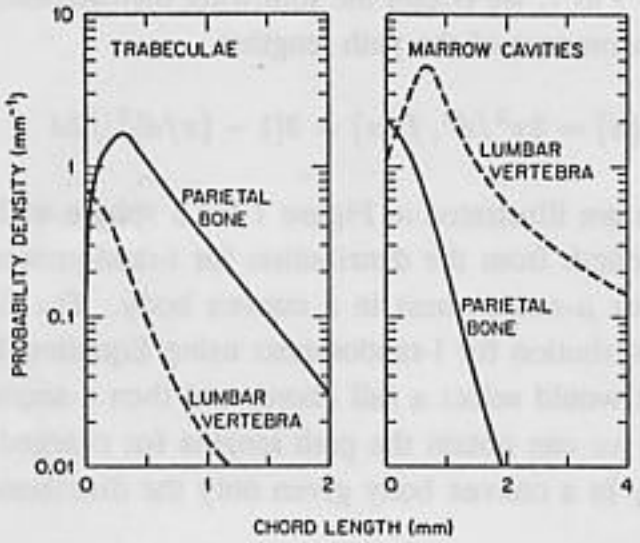

Figure 3. Illustration of measured chord-length distributions for μ-randomness in the bone trabeculae (left) and marrow cavities (right) of the lumbar vertebra and parietal bone from a 44-year-old male

by a straight line, and the absorbed fraction is calculated using chord-length distributions obtained from measurements which satisfy the conditions for μ-randomness (Figure 3). Such measurements for sets of up to nine bones in several species have been reported and applied by Spiers and coworkers in the dosimetry of beta-particle emitters fixed in bone.[7−10] By use of chord-length distributions, the three-dimensional geometry of the calculations is reduced to one dimension. The heterogeneous two-media nature of the problem is also reduced to a single medium by use of the "relative linear stopping power," S, defined as a ratio of the thickness of a reference material to another material for equal energy loss.[21] We use relative linear stopping power (active marrow to trabecular bone) to convert the track length in bone

trabeculae to equivalent track lengths in active marrow, and then use range-versus-energy relationships for active marrow to follow the energy deposition of the charged particle. The range-versus-energy relationships for electrons and heavier charged particles are taken from Berger[22] and Armstrong and Chandler,[23] respectively.

For charged particles emitted in the trabecular bone (Figure 2), we start by Monte Carlo selection of a chord length, t, from the distribution for I-randomness in the bone under consideration. A path length, t', is then determined as $t' = \xi t$, where ξ is a random number such that $0 < \xi < 1$. Tracking of the charged particle is continued by alternate Monte Carlo selection of chord lengths from the distributions for μ-randomness in the marrow cavities, c, and bone trabeculae, t. A charged particle with initial kinetic energy T and range in active marrow R is tracked until

$$S[t' + t_1 + t_2 + ...] + [c_1 + c_2 + c_3 + ...] \geq R(T) \tag{10}$$

The energy deposited in the marrow cavities (c) and trabeculae (t) is calculated as the difference between the residual kinetic energy of the charged particle upon entering and leaving a trabecula or cavity. By tracking a large number of charged particles and calculating their total energy deposition in active marrow, we obtain the absorbed fraction ϕ(RM ← TB).

For charged particles emitted in the marrow cavities (Figure 2), we start by selecting a chord length, c, from the distribution for I-randomness in the marrow cavities, and then a path length c' as discussed above. The tracking of the charged particle continues until

$$[c' + c_1 + c_2 + ...] + S[t_1 + t_2 + t_3 + ...] \geq R(T) \tag{11}$$

The absorbed fraction ϕ(RM ← RM) for self-irradiation of the active marrow is determined also as disucssed above. Typically, 10,000 to 70,000 charged particles were tracked to obtain fractional standard deviations of less than a few percent in each Monte Carlo calculation of the two absorbed fractions.

We have developed absorbed-fraction data for seven bone regions of the skeleton from a 44-year-old male: parietal bone, lumbar vertebra, cervial vertebra, iliac crest, rib, and both the head and neck of the femur.[24] The lumbar vertebra appears, however, to be representative of all marrow sites except those in parietal bone of the skull. Results of our calculations for monoenergetic electrons and protons emitted uniformly in parietal bone and lumbar vertebra are shown in Figures 4 and 5. Note that ϕ(RM ← TB) approaches zero and ϕ(RM ← RM) approaches one at very low electron and proton energies. This limiting behavior occurs because the ranges of the electrons and protons are small relative to the mean path lengths, $\langle t' \rangle_i$ and $\langle c' \rangle_i$, and their energy is deposited locally. At very high electron and i proton energies, we find that

$$\phi(RM \leftarrow TB) = \phi(RM \leftarrow RM) = \frac{< c >_\mu}{< c >_\mu + S < t >_\mu} \tag{12}$$

or the absorbed fractions are equal to the fractional track length in the marrow cavities. Electrons and protons with high energies traverse numerous bone trabeculae and marrow

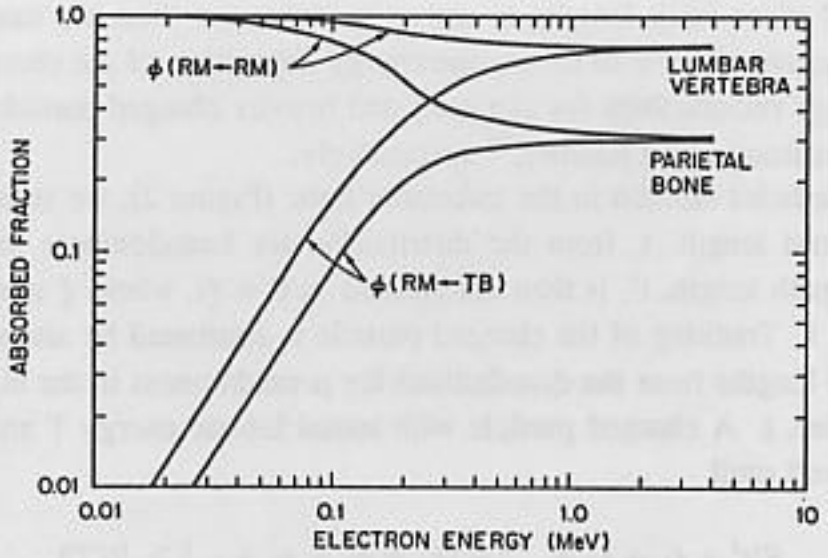

Figure 4. Absorbed fractions for active marrow from monoenergetic electrons emitted uniformly in the trabecular bone, $\phi(RM \leftarrow TB)$, and active marrow, $\phi(RM \leftarrow RM)$, of an adult skeleton

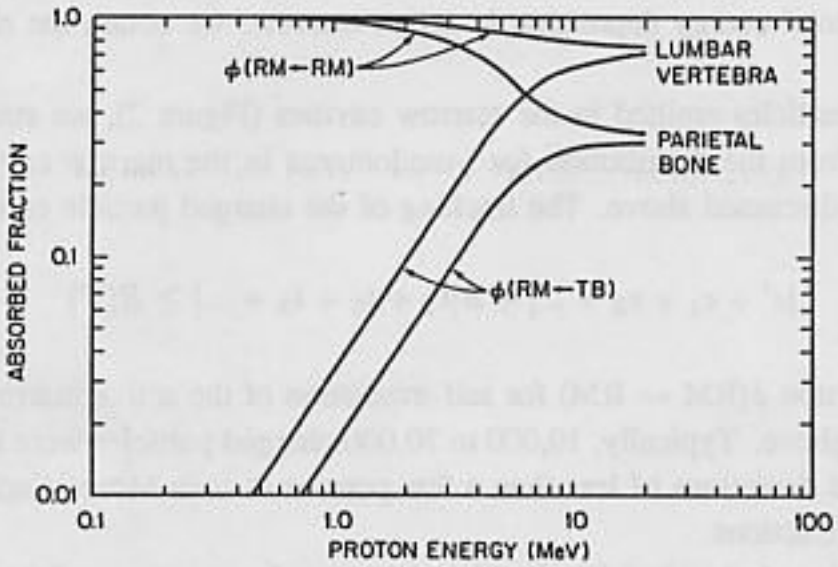

Figure 5. Absorbed fractions for active marrow from monoenergetic protons emitted uniformly in the trabecular bone, $\phi(RM \leftarrow TB)$, and active marrow, $\phi(RM \leftarrow RM)$, of an adult skeleton

cavities, and energy depositions within the active marrow is essentially independent of their origin.

Fluence-to-dose Conversion Factors

The general equation for calculating the absorbed dose, D, in target volume v is:[18,19]

$$D(v) = \frac{1}{m(v)} \sum_{j,r} \phi_j(v \leftarrow r) \Delta_j(r) \tag{13}$$

where $\phi_j(v \leftarrow r)$ = the absorbed fraction in target volume v for charged particles from a photon (or neutron) interaction of kind j in source

region r,
$\Delta_j(r)$ = the total kinetic energy of the charged particles from interaction j in source region r, and
m(v) = the mass of target volume v.

Because our absorbed fractions are developed for monoenergetic charged particles, the above equations is written as

$$D(v) = \frac{1}{m(v)} \sum_{j,r} \int \phi_j(v \leftarrow r) T N_j(r, T) dT \tag{14}$$

where $N_j(r,T)\ dT$ = the absolute number of charged particles with kinetic energies between T and T + dT from interaction j in souce region r.

Since the hematopoietic stem cells at risk are distributed throughout the active marrow, the mean absorbed dose is the appropriate quantity to calculate.[20] We are calculating a mean absorbed dose because our absorbed fractions were averaged over the volume of the active marrow.

If a trabecular bone experiences a fluence, ψ, of photons (or neutrons) of energy E, then we can write

$$N_j(r, T) dT = m(r) \frac{\mu}{\rho}(r, E)_j\ \psi(E) n_j(r, E, T) dT \tag{15}$$

where $n_j(r,E,T)$ = the secondary electron spectrum per interaction j at photon energy E in source region r,
$\frac{\mu}{\rho}(r,E)_j$ = the mass attenuation coefficients for the photoelectric effect (j = 1), Compton effect (j = 2), and pair production (j = 3) at photon energy E in source region r, and
m(r) = the mass of source region r.

By use of Equations 13 to 15, the fluence-to-dose conversion factor for photons of energy E is obtained as

$$\frac{D(v)}{\psi(E)} = \sum_r \frac{m(r)}{m(v)} \sum_j \frac{\mu}{\rho}(r, E)_j \int \phi(v \leftarrow r) n_j(r, E, T) T\ dT \tag{16}$$

This equation can also be applied to neutrons by replacing μ/ρ for photons by σ/ρ, where ρ is the density of source region r and σ is the macroscopic cross section for a neutron interaction of kind j in source region r. If the outer summation is limited to r = RM, and ϕ(RM ← RM) is set equal to one, then we obtain fluence-to-kerma conversion factors for active marrow, v = RM. For r = RM, the value of m(r)/m(v) is one, and for r = TB, we obtain the following relationship by applying Cauchy's theorem (Equation 2) and the equality in surface areas of the marrow cavities and trabecular bone as a boundary condition:

$$m(TB)/m(RM) = [\rho_{TB}/\rho_{RM}][< t >_\mu / < c >_\mu] \tag{17}$$

Table 1. Neutron and Photon Fluence-to-kerma Conversion Factors for Active Marrow

Photon energy (MeV)	Kerma factor (Gy m^2)	Neutron energy (Mev)	Kerma factor (Gy m^2)	Neutron energy (MeV)	Kerma factor (Gy m^2)	Neutron energy (Mev)	Kerma factor (Gy m^2)	Neutron energy (MeV)	Kerma factor (Gy m^2)
1.0E-2[a]	6.04E-16	2.53E-8	2.49E-17	8.60E-2	6.15E-16	5.80E-1	1.81E-15	3.50E+0	4.43E-15
1.5E-2	2.54E-16	3.60E-8	2.11E-17	9.00E-2	6.34E-16	6.20E-1	1.87E-15	3.70E+0	4.50E-15
2.0E-2	1.37E-16	6.30E-8	1.60E-17	9.40E-2	6.53E-16	6.60E-1	1.93E-15	3.90E+0	4.46E-15
3.0E-2	5.95E-17	1.10E-7	1.21E-17	9.80E-2	6.71E-16	7.00E-1	1.99E-15	4.20E+0	4.53E-15
4.0E-2	3.68E-17	2.00E-7	8.96E-18	1.05E-1	7.03E-16	7.40E-1	2.04E-15	4.60E+0	4.51E-15
5.0E-2	2.93E-17	3.60E-7	6.68E-18	1.15E-1	7.47E-16	7.80E-1	2.10E-15	5.00E+0	4.69E-15
6.0E-2	2.77E-17	6.30E-7	5.06E-18	1.25E-1	7.88E-16	8.20E-1	2.15E-15	5.40E+0	4.65E-15
8.0E-2	3.17E-17	1.10E-6	3.83E-18	1.35E-1	8.27E-16	8.60E-1	2.20E-15	5.80E+0	4.82E-15
1.0E-1	3.97E-17	2.00E-6	2.86E-18	1.45E-1	8.65E-16	9.00E-1	2.26E-15	6.20E+0	5.00E-15
1.5E-1	6.58E-17	3.60E-6	2.15E-18	1.55E-1	9.01E-16	9.40E-1	2.34E-15	6.60E+0	4.99E-15
2.0E-1	9.45E-17	6.30E-6	1.66E-18	1.65E-1	9.35E-16	9.80E-1	2.47E-15	7.00E+0	5.14E-15
3.0E-1	1.53E-16	1.10E-5	1.33E-18	1.75E-1	9.68E-16	1.05E+0	2.53E-15	7.40E+0	5.45E-15
4.0E-1	2.09E-16	2.00E-5	1.11E-18	1.85E-1	9.99E-16	1.15E+0	2.55E-15	7.80E+0	5.60E-15
5.0E-1	2.63E-16	3.60E-5	1.06E-18	1.95E-1	1.03E-15	1.25E+0	2.66E-15	8.20E+0	5.45E-15
6.0E-1	3.14E-16	6.30E-5	1.18E-18	2.10E-1	1.07E-15	1.35E+0	2.75E-15	8.60E+0	5.51E-15
8.0E-1	4.09E-16	1.10E-4	1.56E-18	2.30E-1	1.13E-15	1.45E+0	2.82E-15	9.00E+0	5.73E-15
1.0E+0	4.95E-16	2.00E-4	2.43E-18	2.50E-1	1.18E-15	1.55E+0	2.89E-15	9.40E+0	5.88E-15
1.5E+0	6.81E-16	3.60E-4	4.10E-18	2.70E-1	1.24E-15	1.65E+0	2.99E-15	9.80E+0	5.88E-15
2.0E+0	8.33E-16	6.30E-4	6.90E-18	2.90E-1	1.29E-15	1.75E+0	3.05E-15	1.05E+1	5.98E-15
3.0E+0	1.09E-15	1.10E-3	1.19E-17	3.10E-1	1.34E-15	1.85E+0	3.16E-15	1.15E+1	6.33E-15
4.0E+0	1.32E-15	2.00E-3	2.13E-17	3.30E-1	1.38E-15	1.95E+0	3.20E-15	1.25E+1	6.46E-15
5.0E+0	1.54E-15	3.60E-3	3.79E-17	3.50E-1	1.43E-15	2.10E+0	3.32E-15	1.35E+1	6.69E-15
6.0E+0	1.74E-15	6.30E-3	6.51E-17	3.70E-1	1.47E-15	2.30E+0	3.39E-15	1.45E+1	6.98E-15
8.0E+0	2.13E-15	1.10E-2	1.10E-16	3.90E-1	1.53E-15	2.50E+0	3.52E-15	1.55E+1	7.26E-15
1.0E+1	2.52E-15	2.00E-2	1.91E-16	4.20E-1	1.64E-15	2.70E+0	3.69E-15	1.65E+1	7.43E-15
1.5E+1	3.51E-15	3.60E-2	3.17E-16	4.60E-1	1.68E-15	2.90E+0	3.89E-15	1.75E+1	7.52E-15
2.0E+1	4.54E-15	6.30E-2	4.92E-16	5.00E-1	1.68E-15	3.10E+0	3.95E-15	1.85E+1	7.64E-15
		8.20E-2	5.94E-16	5.40E-1	1.75E-15	3.30E+0	4.29E-15	1.95E+1	7.75E-15

[a] Read as 1.0×10^{-2} or 0.010, etc.

Table 2. Dose Conversion Factors for Active Marrow in Parietal Bone (PB) and Lumbar Vertebra (LV)

Photon energy (Mev)	Dose factor (Gy m^2)		Neutron energy (Mev)	Dose factor (Gy m^2)		Neutron energy (MeV)	Dose factor (Gy m^2)	
	PB	LV		PB	LV		PB	LV
1.0E-2	6.30E-16	6.14E-16	5.00E-1[a]	1.67E-15	1.68E-15	3.30E+0	4.00E-15	4.20E-15
1.5E-2	2.71E-16	2.61E-16	5.40E-1	1.73E-15	1.74E-15	3.50E+0	4.10E-15	4.32E-15
2.0E-2	1.53E-16	1.43E-16	5.80E-1	1.79E-15	1.80E-15	3.70E+0	4.14E-15	4.39E-15
3.0E-2	7.49E-17	6.44E-17	6.20E-1	1.85E-15	1.86E-15	3.90E+0	4.07E-15	4.34E-15
4.0E-2	5.04E-17	4.11E-17	6.60E-1	1.92E-15	1.93E-15	4.20E+0	4.09E-15	4.39E-15
5.0E-2	4.18E-17	3.31E-17	7.00E-1	1.97E-15	1.98E-15	4.60E+0	4.00E-15	4.35E-15
6.0E-2	3.93E-17	3.11E-17	7.40E-1	2.02E-15	2.03E-15	5.00E+0	4.11E-15	4.51E-15
8.0E-2	4.15E-17	3.45E-17	7.80E-1	2.08E-15	2.09E-15	5.40E+0	4.02E-15	4.45E-15
1.0E-1	4.79E-17	4.22E-17	8.20E-1	2.12E-15	2.14E-15	5.80E+0	4.12E-15	4.60E-15
1.5E-1	7.16E-17	6.74E-17	8.60E-1	2.17E-15	2.19E-15	6.20E+0	4.23E-15	4.76E-15
2.0E-1	9.88E-17	9.57E-17	9.00E-1	2.23E-15	2.25E-15	6.60E+0	4.16E-15	4.73E-15
3.0E-1	1.57E-16	1.54E-16	9.40E-1	2.31E-15	2.33E-15	7.00E+0	4.25E-15	4.86E-15
4.0E-1	2.15E-16	2.10E-16	9.80E-1	2.44E-15	2.46E-15	7.40E+0	4.50E-15	5.15E-15
5.0E-1	2.72E-16	2.66E-16	1.05E+0	2.49E-15	2.52E-15	7.80E+0	4.59E-15	5.28E-15
6.0E-1	3.28E-16	3.19E-16	1.15E+0	2.51E-15	2.54E-15	8.20E+0	4.40E-15	5.12E-15
8.0E-1	4.28E-16	4.15E-16	1.25E+0	2.61E-15	2.65E-15	8.60E+0	4.41E-15	5.16E-15
1.0E+0	5.19E-16	5.03E-16	1.35E+0	2.70E-15	2.74E-15	9.00E+0	4.59E-15	5.36E-15
1.5E+0	7.13E-16	6.91E-16	1.45E+0	2.75E-15	2.80E-15	9.40E+0	4.70E-15	5.50E-15
2.0E+0	8.79E-16	8.50E-16	1.55E+0	2.82E-15	2.87E-15	9.80E+0	4.66E-15	5.49E-15
3.0E+0	1.17E-15	1.12E-15	1.65E+0	2.91E-15	2.97E-15	1.05E+1	4.69E-15	5.56E-15
4.0E+0	1.43E-15	1.37E-15	1.75E+0	2.96E-15	3.03E-15	1.15E+1	4.97E-15	5.88E-15
5.0E+0	1.69E-15	1.59E-15	1.85E+0	3.06E-15	3.13E-15	1.25E+1	5.04E-15	5.99E-15
6.0E+0	1.94E-15	1.82E-15	1.95E+0	3.08E-15	3.17E-15	1.35E+1	5.22E-15	6.19E-15
8.0E+0	2.46E-15	2.26E-15	2.10E+0	3.19E-15	3.28E-15	1.45E+1	5.47E-15	6.47E-15
1.0E+1	2.99E-15	2.70E-15	2.30E+0	3.23E-15	3.34E-15	1.55E+1	5.72E-15	6.74E-15
1.5E+1	4.38E-15	3.85E-15	2.50E+0	3.34E-15	3.47E-15	1.65E+1	5.86E-15	6.89E-15
2.0E+1	5.87E-15	5.05E-15	2.70E+0	3.49E-15	3.63E-15	1.75E+1	5.93E-15	6.97E-15
			2.90E+0	3.66E-15	3.82E-15	1.85E+1	6.03E-15	7.08E-15
			3.10E+0	3.68E-15	3.87E-15	1.95E+1	6.13E-15	7.19E-15

[a] Use kerma factors from Table 1 at neutron energies below 0.5 MeV.

A value of two was used for the ratio of the densities of trabecular bone to active marrow.

We have investigated both kerma and dose conversion factors for active marrow using the photon cross-section data for discrete energies from Hubbell,[25] the neutron kerma data averaged over given energy intervals from Caswell et al,[26] and the tissue composition data from Kerr.[27] The results are given in Tables 1 and 2. In our photon calculations, we assumed that the photoelectrons have discrete energies equal to the photon energy E. The energy distribution of the Compton electrons was calculated from the Klein-Nishina relationship,[21] and the positron-electron energy distribution was derived from the Bethe-Heitler theory of pair production.[28] Although some differences exist in the energy deposition of electrons and positrons, they are small enough to be disregarded,[22] and the electron absorbed-fraction data were applied to positrons. In our neutron calculations, we considered only the effects of the microstructure of trabecular bone on the absorbed dose in active marrow from elastic scattering of neutrons by hydrogen. The recoil protons were assumed to have a uniform distribution of kinetic energies from the neutron energy E down to zero.[16] For secondary charged particles produced in neutron interactions with other elements, we also assumed that ϕ(RM ← RM) is one and ϕ(RM ← TB) is zero, or that the energy is deposited locally.[6,29] At fast neutron energies between 10 keV and 1 MeV, the proton recoils from elastic scattering of neutrons by hydrogen contribute 90 % or more to total kerma in active marrrow. However, the recoil-proton contribution drops to about 80 % at 10 MeV and about 65 % at 20 MeV.[26,29] In the future, we plan to (a) track additional secondary charged particles from other neutron interactions in our absorbed-dose calculations for active marrow, (b) investigate the dose conversion factors for active marrow of young children, and (c) extend our calculations for neutrons and photons to the endosteum of the marrow cavities. The endosteal surfaces of both trabecular and cortical bone contain the osteogenic cells which are considered as the critical targets for induction of bone cancer.[20]

Discussion

Absorbed dose (i.e., energy deposited by charged particles) and kerma (i.e., kinetic energy released in matter) can be equated in most soft tissues of the body.[27] However, the soft tissues in bone receive secondary charged particles from the bone, and absorbed dose and kerma may not be equal (Figure 6). The absorbed dose is smaller for fast neutrons because of the hydrogen deficiency in bone and larger than kerma for low energy photons because of the enhanced photoelectron production in bone. Enhancement of the absorbed dose at high photon energies from pair production in bone is also indicated by our calculations. Our results are presented as neutron and photon fluence-to-dose conversion factors which can be applied in radiation transport calculations using anthropomorphic phantoms with a homogeneous representation of the skeleton.[30–32] While the homogenized skeleton provides appropriate radiation transport characteristics, it ignores effects of the microstructure of trabecular bone on absorbed dose in active marrow.[33] We find that the dose conversion factors for lumbar vertebrae can be used as a representative example for all active marrow sites except those in parietal bone.[24] Hence, our recommendation is that only the parietal bone be treated separately from other bone regions in radiation transport calculations of absorbed dose in active marrow of the body. The absorbed dose in active marrow of parietal bone is significantly different from that in other bones of the body, and the parietal bone of

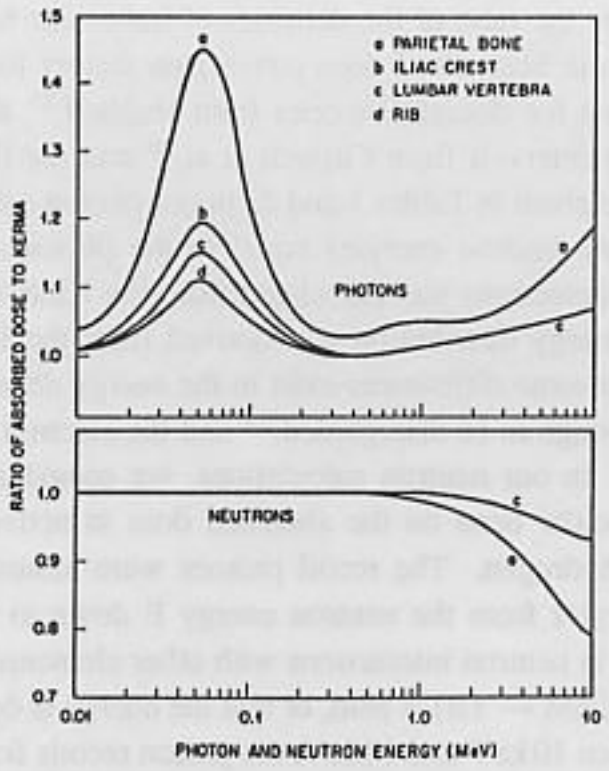

Figure 6. Illustration of the effects of the microstructure of trabecular bone on energy deposition in active marrow of an adult skeleton

young children contains a surprisingly large fraction of the total active marrow.[32] Results of this study are now being used in the reassessment of organ doses for A-bomb survivors in Hiroshima and Nagasaki.[34]

References

1. International Commission on Radiation Units and Measurements, 1969. *Clinical Dosimetry*. Bethesda, MD: ICRU, report 10d, National Bureau of Standards handbook 87.
2. Spiers, F. W., 1969. Transition-zone dosimetry. In *Radiation Dosimetry*, vol. 3, F. H. Attix and E. Tochilin, Eds., pp.809-867. New York: Academic Press.
3. Sinclair, W. K., 1969. Radiobiological dosimetry. In *Radiation Dosimetry*, vol. 3, F. H. Attix and E. Tochilin, Eds., pp.617-676. New York: Academic Press.
4. Lawson, R. C., 1967. The recoil proton dose at a bone-tissue interface irradiated by fast neutrons. Phys. Med. Biol. 12:551-554.
5. Prasad, M. A., Sundararaman, V., and Venkataraman, G., 1971. The recoil proton dose across a bone-tissue interface due to neutrons. Phys. Med. Biol. 16:461-466.
6. Bhatia, D. P. and Nagarajan, P. S., 1979. Fast neutron dosimetry of a bone-tissue interface. Phys. Med. Biol. 24:166-170
7. Beddoe, A. H., 1978. A quantitative study of the structure of trabecular bone in man, rhesus monkey, beagle and miniature pig. Calcif. Tiss. Res. 25:273-282.
8. Beddoe, A. H., Darley, P. J., and Spiers, F. W., 1976. Measurements of trabecular bone structure in man. Phys. Med. Biol. 21:589-607.
9. Whitwell, J. R. and Spiers, F. W., 1976. Calculated beta-ray dose factors for trabecular bone. Phys. Med. Biol. 21:16-38.

10. Whitwell, J. R., 1973. Theoretical *Investigations of Energy Loss by Ionizing Particles in Bone*. Leeds: University of Leeds, Ph.D. thesis.

11. Kellerer, A. M., 1981. Concepts of geometrical probability relevant to microdosimetry and dosimetry. In *Seventh Symp. on Microdosimetry*, pp. 1049-1065. London: Harwood Academic Publishers.

12. Kellerer, A. M., 1971. Considerations on the random traversal of convex bodies and solutions for general cylinders. Radiat. Res. 47:359-376

13. Kendall, M. G. and Morgan, P. A. P., 1963. *Geometrical Probability*. New York: Hafner Publishing Co.

14. Coleman, R., 1969. Random paths through convex bodies. J. Appl. Prob. 6:430-441.

15. Kingman, J. F. C., 1965. Mean free paths in a convex reflecting region. J. Appl. Prob. 2:162-168.

16. Caswell, R. S., 1966. Deposition of energy by neutrons in spherical cavities. Radiat. Res. 27:92-107.

17. Rossi, H. H. and Rosenzweig, W., 1955. A device for the measurement of dose as a function of specific ionization. Radiology 64:404-411.

18. Loevinger, R., 1969. Distributed radionuclide sources. In Radiation Dosimetry, vol. 3, F. H. Attix and E. Tochilin, Eds., pp. 51-90. New York: Academic Press.

19. International Commission on Radiation Units and Measurements, 1979. *Method of Assessment of Absorbed Dose in Clinical Use of Radionuclides. Bethesda, MD: ICRU, report 32.*

20. *International Commission on Radiation Protection, 1967. A Review of the Radiosensitivity of the Tissues in Bone*. Oxford: Pergamon Press, ICRP, publication 11.

21. Evans, R. D., 1955. *The Atomic Nucleus*. New York: Academic Press.

22. Berger, M. J., 1973. *Improved Point Kernels for Electron and Beta-Ray Dosimetry*. Washington: National Bureau of Standards, report NBSIR-73- 107.

23. Armstrong, T. W., and Chandler, K. C., 1973. *SPAR, A Fortran Program for Computing Stopping Powers and Ranges for Muons, Charged Pions, Protons and Heavy Ions*. Oak Ridge, TN: Oak Ridge National Laboratory, report ORNL-4869.

24. Eckerman, K. F. and Cristy, M., 1984. Computational method for realistic estimates of the dose to active marrow.. In *Radiation-Risk-Protection*, A. Kaul, R. Neider, J. Pensko, F.-F. Stieve, and H. Bunner, Eds., vol. 3, pp. 984-987. Julich: Fachverband fur Strahlenschutz.

25. Hubbell, J. H., 1982. Photon mass attenuation and energy-absorption coefficients from 1 keV to 20 MeV. Int. J. Appl. Radiat. Isot. 33:1269-1290.

26. Caswell, R. S., Coyne, J. J., and Randolph, M. L., 1980. Kerma factors for neutron energies below 30 MeV. Radiat. Res. 83:217-254.

27. Kerr, G. D., 1982. *Photon and Neutron Fluence-to-Kerma Factors for ICRP-1975 Reference Man Using Improved Elemental Compositions for Bone and Marrow of the Skeleton*. Oak Ridge, TN: Oak Ridge National Laboratory, report ORNL/TM-8318.

28. Hough, P. V. C., 1948. Low energy pair production. Phys. Rev. 73:266-267.

29. International Commission on Radiation Units and Measurements, 1977. *Neutron Dosimetry for Biology and Medicine*. Bethesda, MD: ICRU, report 26.

30. Snyder, W. S., Ford, M. R., Warner, G. G., and Fisher, H. L., 1969. Estimates of absorbed fractions for monoenergetic photon sources uniformly distributed in various organs of a heterogeneous phantom. J. Nucl. Med., supplement 3.

31. Cristy, M., 1980. *Mathematical Phantoms Representing Children of Various Ages for Use in Estimates of Internal Dose*. Oak Ridge, TN: Oak Ridge National Laboratory, report ORNL/NUREG/TM-367.

32. Cristy, M., 1981. Active bone marrow distribution as a function of age in humans. Phys. Med. biol. 26:389-400.

33. Kerr, G. D., 1980. A review of organ doses from isotropic fields of gamma rays. Health Physics 39:3-20.

34. Kerr, G. D., 1981. Review of dosimetry for the atomic bomb survivors. In *Fourth Symp. on Neutron Dosimetry, stmr vol. 1, pp. 501-513. Luxembourg: Commission of the European Communities.*